

# An exploratory investigation of the high pressure $\beta$ - $V_2O_5$ polymorph as 3 V cathode material for potassium-ion battery

Ankush Bhatia<sup>a,\*</sup>, Jean-Pierre Pereira-Ramos<sup>a</sup>, Maria Elena Arroyo-de Dompablo<sup>b</sup>, Rita Baddour-Hadjean<sup>a,\*</sup>

<sup>a</sup> Institut de Chimie et des Matériaux Paris Est (ICMPE), UMR 7182 CNRS-Université Paris Est Créteil, 2 rue Henri Dunant, 94320 Thiais, France

<sup>b</sup> Departamento de Química Inorgánica, Universidad Complutense de Madrid, Madrid 28040, Spain

## ARTICLE INFO

### Keywords:

High pressure  $\beta$ - $V_2O_5$   
Layered structure  
K-ion battery  
Positive electrode

## ABSTRACT

Electrochemical potassium-ion insertion in high pressure /high temperature (HP/HT)  $\beta$ - $V_2O_5$  polymorph is examined for the first time. Monoclinic HP/HT  $\beta$ - $V_2O_5$  delivers a high reversible capacity of 120 mAh g<sup>-1</sup> at C/20 rate corresponding to the  $K_{0.8}V_2O_5$  composition, at an average discharge potential of 3.2 V vs.  $K^+/K$ . A good cycling performance is achieved over at least 175 cycles at C/5 rate at room temperature, confirming HP/HT  $\beta$ - $V_2O_5$  is an efficient host material for  $K^+$  insertion-extraction reaction. First insight into the reversibility of the structural changes upon potassiation is given.

## 1. Introduction

Potassium-ion batteries (KIBs) have garnered significant attention in the field of electrochemical energy storage. This is primarily due to the following key factors: the negative standard potential of  $K^+/K$  couple ( $-2.93$  V vs. SHE), lower than that of  $Na^+/Na$  system resulting in high operating potential of potassium-based cathode materials as compared to sodium-based alternatives, the potassium abundance in the earth's crust which is nearly equivalent to that of sodium resources, and possibility of the reversible (de)intercalation of K-ions into the graphite anode [1,2]. These advantages have contributed to the growing interest in exploring the potential of KIBs for practical applications in energy storage [3,4]. However, the large ionic radius of  $K^+$  ( $K^+ > Na^+ > Li^+$ ,  $1.38 > 1.02 > 0.76$  Å in terms of ionic radius) and the large volume changes induced by  $K^+$  accommodation have limited practical application. Therefore, the search for suitable cathode materials remains a crucial challenge in unlocking the full potential of KIBs.

There is ample space available for the exploration and advancement of K-ion cathode materials, with a specific emphasis on layered oxides. The rich redox chemistry of vanadium has led to important interest in  $V_2O_5$  owing to its high theoretical capacity for metal-ion batteries [5]. Variety of K-containing V-based oxides (KVO) such as electroformed  $K_xV_2O_5$  ( $0 < x < 0.6$ ) obtained from  $\alpha$ - $V_2O_5$  in potassiated-dimethylsulfone electrolyte at 150 °C [6], bilayered  $\delta$ - $K_{0.5}V_2O_5$  [7],  $K_{0.83}V_2O_5$  chemically synthesized by soft chemistry [8]

and some hydrated phases such as  $V_2O_5 \cdot 0.6-0.8H_2O$  [9,10],  $K_{0.42}V_2O_5 \cdot 0.25H_2O$  [11] have been reported as promising cathode materials for KIBs. High specific energy and excellent cycling stability make also V-based polyanionic and Prussian blue analogues attractive cathode materials for K storage [3,12–14]. However, only a few papers have focused on the K-storage properties of  $\alpha$ - $V_2O_5$  at room temperature (RT) in standard organic based-electrolytes. Q. Fu *et al.*, [15] in 2021 reported the potassium insertion in orthorhombic nanosized  $\alpha$ - $V_2O_5$  prepared by hydrothermal route. An initial potassiation/depotassiation capacity of 200 mAhg<sup>-1</sup> (1.36  $K^+$  ions) at a low potential of 1.7 V vs.  $K^+/K$  was displayed with a rapid capacity decline reaching 54 mAhg<sup>-1</sup> at the 31st cycle. Further, using specific electrode design, crystalline  $\alpha$ - $V_2O_5$  nanorods@rGO [16] and amorphous  $\alpha$ - $V_2O_5$ @CNT [17] were reported as host material for potassium insertion delivering capacity ranging between 50 and 200 mAh g<sup>-1</sup>. However, both of these tailored orthorhombic  $\alpha$ - $V_2O_5$  oxides operate at a low discharge potential of around 1.8 V vs.  $K^+/K$ . As a proof of concept, our group has recently extended  $K^+$  insertion to another  $V_2O_5$  polymorph called  $\gamma$ '- $V_2O_5$  with attractive electrochemical features [18]. A high amount of potassium (up to 0.9  $K^+$  mol<sup>-1</sup> in the 4.4 – 1.5 V voltage window) can be electrochemically accommodated between the puckered layers of  $\gamma$ '- $V_2O_5$  at a high discharge potential of  $\approx 3.3$  V vs.  $K^+/K$  (twofold higher compared to  $\alpha$ - $V_2O_5$ ) with a stable specific capacity of  $\sim 50-60$  mAhg<sup>-1</sup>.

Looking at other  $V_2O_5$  polymorphs, a few papers outline the potential interest of the layered high pressure/high temperature (HP/HT)  $\beta$ - $V_2O_5$

\* Corresponding authors.

E-mail addresses: [ankush\\_bhatia34@yahoo.com](mailto:ankush_bhatia34@yahoo.com) (A. Bhatia), [rita.baddour-hadjean@cnrs.fr](mailto:rita.baddour-hadjean@cnrs.fr) (R. Baddour-Hadjean).

<https://doi.org/10.1016/j.electacta.2024.144311>

Received 16 February 2024; Received in revised form 14 April 2024; Accepted 22 April 2024

Available online 23 April 2024

0013-4686/© 2024 Elsevier Ltd. All rights reserved.

polymorph as host lattice for electrochemical insertion reactions. In 2007, Arroyo-de Dompablo *et al.* [19], showed promising  $\text{Li}^+$  insertion capabilities of the  $\beta\text{-V}_2\text{O}_5$  polymorph delivering a first discharge capacity of  $240 \text{ mAh g}^{-1}$  near 3.2 V vs.  $\text{Li}^+/\text{Li}$ , leading to  $\beta\text{-Li}_{1.6}\text{V}_2\text{O}_5$  with stable cycling behavior over at least 27 cycles in the 4 V – 1 V voltage range. Interestingly, Cordoba *et al.* [20], recently reported  $\text{Na}^+$  insertion in  $\beta\text{-V}_2\text{O}_5$  at a high potential of  $\approx 3 \text{ V}$  vs.  $\text{Na}^+/\text{Na}$  delivering a capacity of  $132 \text{ mAh g}^{-1}$  ( $\beta\text{-Na}_{0.9}\text{V}_2\text{O}_5$ ) in the 3.6–2.0 V range. However, due to irreversible phase transformations not yet solved, the specific capacity was reported to decrease continuously in the first few cycles before reaching a stable value of  $75 \text{ mAh g}^{-1}$  at C/10 rate. Very recently, Trocoli *et al.* [21], reported an extension of  $\beta\text{-V}_2\text{O}_5$  insertion properties to the case of magnesium intercalation. Their study used a combination of several characterization techniques to give evidence for the structural changes associated with the  $\text{Mg}^{2+}$  (de-) intercalation. A specific capacity of  $350 \text{ mAh g}^{-1}$  was reported on the first discharge corresponding to the  $\beta\text{-Mg}_{1.2}\text{V}_2\text{O}_5$  composition, but at a low working potential of  $\approx 1.4 \text{ V}$  vs.  $\text{K}^+/\text{K}$  pointing a difficult magnesium accommodation probably due to the high charge density of  $\text{Mg}^{2+}$ . These previous data on lithium, sodium and magnesium insertion in  $\beta\text{-V}_2\text{O}_5$  motivated us to explore for the first time the electrochemical potassium intercalation characteristics in this high pressure  $\text{V}_2\text{O}_5$  polymorph.

## 2. Material and methods

$\beta\text{-V}_2\text{O}_5$  was prepared according to the protocol described by Arroyo-de Dompablo *et al.* [22,23] by subjecting commercial (Aldrich)  $\alpha\text{-V}_2\text{O}_5$  at a high pressure of 4 GPa and at temperature of 800 °C in a Conac press. After the pressure and temperature were applied for 0.5 h, the vessel was quenched to RT while the pressure was slowly released. The morphology and elemental composition of the obtained black-reddish powder were characterized by scanning electron microscopy (SEM), (Zeiss, Merlin-type microscope) and electron dispersive X-ray spectroscopy (EDS) analysis together with SEM using an accelerating voltage of 10 – 15 kV.

Crystal structures were determined using X-ray diffraction (XRD) as well as Raman spectroscopy. XRD experiments were performed using a Panalytical XPert pro apparatus equipped with a X'Celerator detector and using  $\text{Co K}\alpha$  radiation ( $\lambda\text{K}\alpha = 1.789 \text{ \AA}$ ). All the diffraction patterns were collected with a 2 $\theta$  step of 0.0167° A He:Ne laser (632.8 nm) was used as the excitation source to record the Raman spectra with a LaB-RAM HR 800 (Jobin-Yvon-Horiba).

Without any further cathode optimization, 80 wt.% of  $\beta\text{-V}_2\text{O}_5$  powder was used to prepare the working electrode by mixing with 7.5 wt.% of acetylene black, 7.5 wt.% of graphite and 5 wt.% of PTFE as binder to make a sheet. This sheet was cut into disc of 0.8 cm in diameter (about 6 mg of active material). Potassium metal was used as counter and reference electrode. The CR2032 two electrode coin-cells were assembled in an argon-filled glove box. The positive electrode (sheet) is separated from the negative electrode (K-metal) by Whatman glass fiber disks soaked in 0.5 M  $\text{KPF}_6/\text{Ethylene carbonate (EC): Propylene carbonate (PC) 1:1 2\% vol. Fluoroethylene carbonate (FEC) electrolyte}$ . Electrochemical tests were carried out at RT using a VMP3 Biologic apparatus. The cells were electrochemically cycled at different c-rates (C/100–1C).

The XRD patterns and Raman spectra of electrochemically formed  $\beta\text{-K}_x\text{V}_2\text{O}_5$  samples have been recorded according to the following *ex situ* procedure. After 2 h of equilibrium time, the positive electrodes were removed from the cell in an Ar-filled glove box, rinsed with DMC, and placed in appropriate airtight sample holders to be analyzed by XRD, using a 2 $\theta$  step of 0.0167° and Raman spectroscopy. Raman spectra were recorded on 10 different spots of each electrode. Similar spectra were recovered for all the investigated points, whatever the electrode, indicating their good homogeneity.

## 3. Results and discussion

Fig. 1a illustrates the morphology of the as-synthesized powder, which consists of tiny platelets of a few hundred nanometers width. The XRD pattern (Fig. 1b) indicates that pure  $\beta\text{-V}_2\text{O}_5$  is obtained with  $P21/m$  monoclinic symmetry and unit cell parameters  $a = 7.1016(3) \text{ \AA}$ ,  $b = 3.5668(1) \text{ \AA}$ ,  $c = 6.2742(3) \text{ \AA}$  and  $\beta = 90.121(3)^\circ$ , in good agreement with the layered crystal structure proposed by V. P. Filonenko and Gallardo-Amores and illustrated in Fig. 1c [22–24].

The Raman spectrum of the as-prepared powder (Fig. 1d) exhibits a series of well-resolved bands assigned to a well-crystallized  $\beta\text{-V}_2\text{O}_5$  sample, in good agreement with that previously reported [25]. The point group symmetry of  $\beta\text{-V}_2\text{O}_5$  is  $C_{2h}$ , and therefore, the crystallographic sites of V,  $\text{O}_1$  and  $\text{O}_2$  atoms split into two nonequivalent positions distinguished by subscripts a and b in Fig. S1. The crystal structure of  $\beta\text{-V}_2\text{O}_5$  is built up of  $[\text{V}_2\text{O}_5]$  units forming infinite chains along the y direction. The chains are linked by corner-sharing octahedra forming layers held together by relatively weak interactions and stacked along the x direction. Three types of V-O bonds can be identified in the units (Fig. S1) [25]: the shortest vanadyl V- $\text{O}_1$  bonds, V- $\text{O}_3$  bonds forming asymmetric V- $\text{O}_3$ -V bridges in the xz plane and V- $\text{O}_2$  bonds forming V- $\text{O}_2$ -V bridges oriented along the y direction. Based on the results of calculations, the Raman peaks of pristine  $\beta\text{-V}_2\text{O}_5$  have been previously assigned to specific vibrational modes taking into account these structural data. The two sharp peaks at 1017 and 937  $\text{cm}^{-1}$  are assigned to the stretching modes of the shortest  $\text{V}_a\text{-O}_{1a}$  and  $\text{V}_b\text{-O}_{1b}$  bonds, respectively. Then, the vibrations of the bridging  $\text{O}_3$  atoms give rise to the  $\text{V}_b\text{-O}_3$  and  $\text{V}_a\text{-O}_3$  stretching modes observed at 739 and 583  $\text{cm}^{-1}$ , respectively. The Raman line at 682  $\text{cm}^{-1}$  corresponds to the asymmetric vibration of  $\text{O}_{2a}$  atoms in the  $\text{V}_a\text{-O}_{2a}\text{-V}_b$  bridge while the band at 472  $\text{cm}^{-1}$  is attributed to the stretching of the  $\text{V}_b\text{-O}_{2a}$  bond. Below 450  $\text{cm}^{-1}$ , several well-resolved peaks are observed, which are mostly assigned to complex vibrations of the  $\text{V}_2\text{O}_5$  chains.

Fig. 2a shows the cyclic voltammogram (CV) of  $\beta\text{-V}_2\text{O}_5$  recorded in the 2.2 – 4.4 V vs.  $\text{K}^+/\text{K}$  voltage range at a sweeping rate of 0.1  $\text{mV s}^{-1}$ . CV curves show two broad cathodic peaks centered at ca. 3.04 V and 2.4 V with a shoulder at 2.84 V and four anodic peaks centered at ca. 3.08 V, 3.48 V, 3.84 V and 4.15 V. Such observations suggest the participation of different structural mechanisms involved during the reduction and oxidation processes. Noteworthy, the same coulombic charge was involved during reduction and oxidation, showing the high efficiency of the electrochemical process. It can be noticed a slight shift in the cathodic peak potentials ( $\sim 100 \text{ mV}$ ) between cycle 1 and 2 showing an easier potassium insertion process induced after a first reduction-oxidation cycle.

In order to get a quasi-equilibrium potential evolution vs. K composition in the electrode, a galvanostatic discharge-charge curve of  $\beta\text{-V}_2\text{O}_5$  electrode was carried out at a low rate of C/100 ( $\sim 1.5 \text{ mA g}^{-1}$ ) in the 2.2 – 4.4 V voltage range (Fig. 2b). Three well-defined insertion steps at 3.4 V, 3.0 V and 2.7 V are clearly evidenced. The first discharge plateau at 3.4 V involves a potassium uptake of 0.32 corresponding to a capacity of  $47 \text{ mAh g}^{-1}$ , and then it is followed by a sloping curve from 3.25 V to 2.7 V with additional 0.28 inserted  $\text{K}^+$  ions ( $41 \text{ mAh g}^{-1}$ ). The last step observed as a flat voltage plateau at 2.7 V involves a potassium uptake of 0.26  $\text{K}^+$  corresponding of a further capacity of  $40 \text{ mAh g}^{-1}$ . The total discharge capacity involved in the reduction process is  $\sim 127 \text{ mAh g}^{-1}$ , leading to a composition of  $\text{K}_{0.85}\text{V}_2\text{O}_5$  for the discharged product. The subsequent charge process includes 4 steps at 2.8 V, 3.5 V, 3.9 V and 4.2 V with a total capacity of  $130 \text{ mAh g}^{-1}$ . This first discharge-charge cycle displays a coulombic efficiency of around 100%. Such results indicate that different mechanisms are probably involved during  $\text{K}^+$  insertion and deinsertion, ensuring however a high rechargeability. Fig. 2b clearly shows the interest provided by the structure of  $\beta\text{-V}_2\text{O}_5$  as host lattice for K insertion since the redox process occurs between 3.48 and 2.2 V vs.  $\text{K}^+/\text{K}$ , i.e.  $\approx 3.28 \text{ V}$  vs.  $\text{Na}^+/\text{Na}$ , which corresponds to the same potential range and potential insertion steps

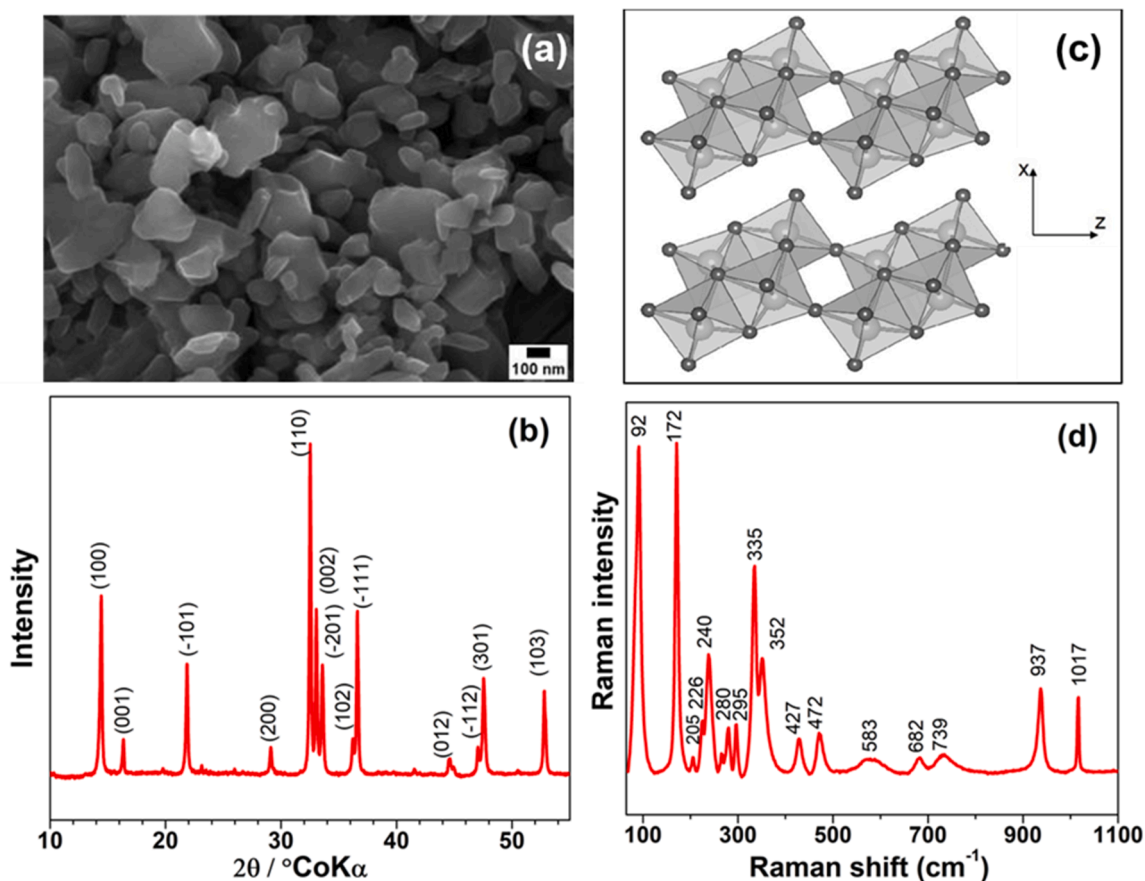


Fig. 1. Characterization of the as prepared  $\beta$ - $V_2O_5$  powder (a) SEM image; (b) X-ray diffraction pattern; (c) Schematic structural representation in the xz projection; (d) Raman spectrum.

previously reported for sodium ions [20]. This result shows that the expected penalty due to the size effect is not observed for potassium accommodation, at least from a thermodynamic point of view. Interestingly, the size effect (or more precisely, the polarizing capability) of the inserted cation seems to be vital if one compares Na/K with Li. As reported by Gallardo et al [19], Li intercalation proceeds throughout six fully reversible reduction/oxidation steps in a wide voltage range (4.2–1 V).

Rate capability tests in the C/20 to 1C range confirm the promising performance of  $\beta$ - $V_2O_5$  electrode. The first discharge-charge cycle of the  $\beta$ - $V_2O_5$  electrode at different current densities is shown in Fig. 2c. A galvanostatic cycle recorded at C/20 rate reveals a discharge capacity of  $120 \text{ mAh g}^{-1}$  at an average discharge potential of 3.1 V. Table 1 shows the results of EDS analysis of the discharged electrodes recovered at two different lower cut off potential (2.6 V and 2.2 V) performed at a C/20 rate. The K/V ratio found from EDS measurements were 0.25 (discharge till 2.6 V) and 0.40 (discharge till 2.2 V), which is consistent with the compositions of  $K_{0.54}V_2O_5$  and  $K_{0.82}V_2O_5$ , respectively. A subsequent charge capacity of  $118 \text{ mAh g}^{-1}$  was obtained with a coulombic efficiency of 99 %. The EDS analysis of the charged electrode gives a K/V ratio of 0.05 ( $K_{0.1}V_2O_5$ ), which is close to the potassium content calculated from the faradaic yield ( $0.06 \text{ F mol}^{-1}$ ). The difference between the remaining amounts of  $K^+$  ions can be explained by a less efficient rinsing procedure for this particular experiment. A strong influence of the current density is observed in the C/20 – C/5 range, suggesting a kinetically hindered intercalation reaction. This is probably due to the slow diffusion of large sized potassium-ion (ionic radius of  $1.38 \text{ \AA}$ ). Indeed, a capacity of  $120 \text{ mAh g}^{-1}$  is reached at C/20 ( $\sim 8 \text{ mA g}^{-1}$ ),  $85 \text{ mAh g}^{-1}$  at C/10 ( $\sim 16 \text{ mA g}^{-1}$ ),  $60\text{--}65 \text{ mAh g}^{-1}$  at C/5 ( $\sim 32 \text{ mA g}^{-1}$ ) and C/2 ( $\sim 80 \text{ mA g}^{-1}$ ), respectively, with still  $50 \text{ mAh g}^{-1}$  obtained at 1C ( $\sim 160 \text{ mA}$

$g^{-1}$ ). These results are very close or higher than those reported for sodiation with capacities of 130, 80 and  $75 \text{ mAh g}^{-1}$  at respectively C/20, C/10 and C/5 and only  $\sim 10 \text{ mAh g}^{-1}$  at 1C [20].

The above rate capability study confirms the attractive properties of  $\beta$ - $V_2O_5$ . Regarding other K-cathode materials,  $\beta$ - $V_2O_5$  well competes with  $\gamma$ - $V_2O_5$  [18] and  $K_xMnO_2/K_xMn_{0.75}Ni_{0.25}O_2$  [26]. The maximum capacity of  $120 \text{ mAh g}^{-1}$  displayed by  $\beta$ - $V_2O_5$  significantly exceeds that exhibited by some bilayered potassium bronzes like  $K_{0.5}V_2O_5$  [7] and  $K_{0.83}V_2O_5$  [8] and is equal to that offered by the best KVO compound, i. e.  $K_{0.5}V_2O_5$  [27], the latter being characterized by a better rate capability.

Galvanostatic cycling experiments of  $\beta$ - $V_2O_5$  composite electrode was also performed at a C/10 rate ( $\sim 16 \text{ mA g}^{-1}$ ) in the same 4.4 V – 2.2 V potential window. As shown in Fig. 3a, starting from the OCV voltage of 3.87 V vs.  $K^+/K$ , the voltage quickly falls down to  $\sim 3.22 \text{ V}$ , then follows a gentle slope till 2.6 V trailing by a second plateau starting at 2.6 V till 2.2 V. A total discharge capacity of c.a.  $85 \text{ mAh g}^{-1}$  ( $0.58 \text{ F mol}^{-1}$ ) is then reached at 2.2 V. Upon subsequent charge of the cell, four steps at 2.9 V, 3.6 V, 4.0 V and 4.35 V are observed involving a total capacity of  $71 \text{ mAh g}^{-1}$  indicating a coulombic efficiency of 84 %. A small amount of  $0.1 \text{ K}^+$  is probably trapped after the first charge. However, on the second cycle, the same discharge/charge capacities of  $85 \text{ mAh g}^{-1}$  are observed, indicating a quantitative charge process. In addition, potassiation of  $\beta$ - $V_2O_5$  seems to be easier since occurring  $\sim 100 \text{ mV}$  higher than in the first cycle (3.1 V vs.  $K^+/K$ ). Further discharge-charge cycles completely superimpose till 5th cycle (Fig. 3b). The different voltage steps in both charge and discharge become less marked, resulting in a reversible S-shape profile with a mid-discharge potential of around 3.2 V. Surprisingly, the width of the second plateau between 2.6 and 2.2 V gradually diminishes with the cycling and

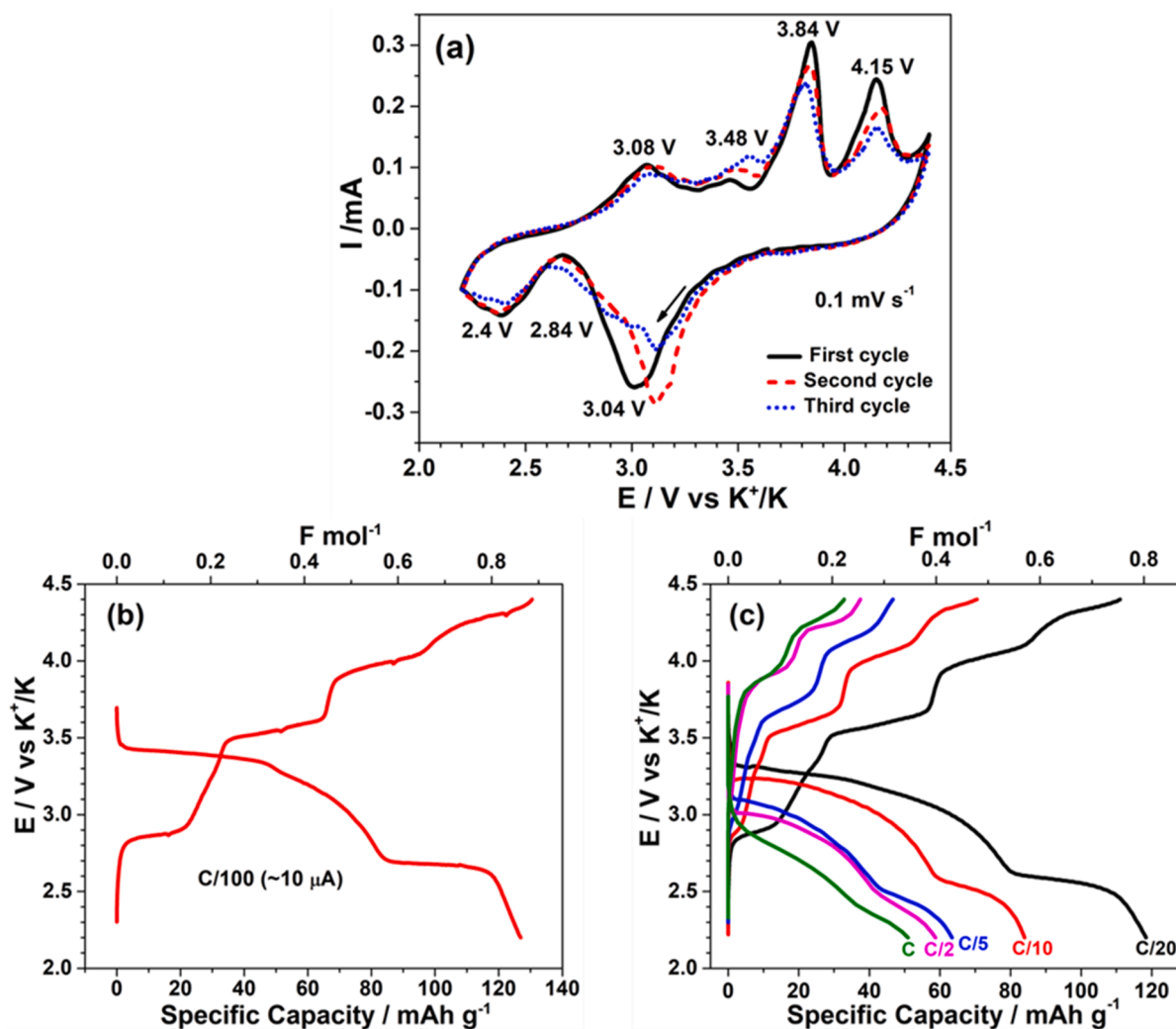


Fig. 2. Electrochemical performance of  $\beta$ - $V_2O_5$  (a) CV curves at  $0.1 \text{ mV s}^{-1}$ ; (b) First discharge-charge cycle at C/100 rate; (c) First discharge-charge cycle at different C-rates. 2.2–4.4 V voltage window. 0.5 M  $KPF_6$  EC: PC + 2 % FEC electrolyte.

Table 1

K/V ratios in different electrodes from EDS analysis and electrochemistry (EC).

Electrode History	F/ mol	x in $K_xV_2O_5$ (EC)	K/V ratio (EDS)	x in $K_xV_2O_5$ (EDS)
1st Discharge till 2.6 V (C/20)	0.54	0.54	0.25	0.5
1st Discharge till 2.2 V (C/20)	0.82	0.82	0.40	0.80
1st Charge till 4.4 V after d-2.2 V (C/20)	0.06	0.06	0.053	0.1

completely disappears from the 10th cycle. This suggests that fewer phase transformations take place upon charge/discharge. Additional analysis of the structural changes is required to understand the underlying cause for this phenomenon.

Fig. 3c illustrates the specific discharge capacities of  $\beta$ - $V_2O_5$  in K cells as a function of the cycle number when cycled at different current densities. The discharge capacity decreases rapidly from  $120 \text{ mAh g}^{-1}$  from the first cycle at C/20 till 20th cycle to reach a stable capacity of  $65 \text{ mAh g}^{-1}$  at 30th cycle. Notably when cycled at C/10 rate, a stable capacity of  $52 \text{ mAh g}^{-1}$  is involved over 120 cycles and still  $43 \text{ mAh g}^{-1}$  are recovered after 175 cycles at C/5 rate. At both C/2 and 1C rate, a lower capacity of  $35 \text{ mAh g}^{-1}$  is achieved after 100 cycles. The present cycling

data show the capacity fading mainly comes from the last step contribution located at 2.5 V at C/10 rate. Fig. S2 shows that by changing the lower cut off voltage from 2.2 V to 2.6 V (to avoid the last insertion step), a better cycling behaviour is obtained. Indeed, the huge capacity fading over the first ten cycles is suppressed. The capacity slowly decreases from 60 to  $50 \text{ mAh g}^{-1}$  after 40 cycles and remains stable at least up to cycle 80. These results serve as a proof of the extraordinary structural stability exhibited by the  $\beta$ - $V_2O_5$  material upon  $K^+$  successive insertion/deinsertion processes, as observed in the case of lithiation [19] but differently from what was reported in the case of sodiation [20].

For comparison, the electrochemical behavior at RT of the conventional micrometric sized  $\alpha$ - $V_2O_5$  polymorph has also been investigated at C/10 rate in the same 4.4 V – 2.2 V potential window, using the same  $KPF_6$  EC: PC electrolyte (Fig. S3). The corresponding cycling behaviour of  $\alpha$ - $V_2O_5$  is reported in Fig. 3c and Fig. S3. In this case, a reversible capacity of only  $4 \text{ mAh g}^{-1}$  is reached at 2.2 V, corresponding to the  $K_{0.04}V_2O_5$  composition, indicating that practically no redox activity occurs upon potassium insertion in micrometric sized  $\alpha$ - $V_2O_5$  polymorph. In the case of a nanosized  $\alpha$ - $V_2O_5$ , [15] a discharge capacity of  $45 \text{ mAh g}^{-1}$  was reported at 2.2 V vs.  $K^+/K$  while the major redox activity was observed at very low voltage of around 1.75 V.

These findings support the remarkable ability of the  $\beta$ - $V_2O_5$  structure to accommodate  $K^+$  ions at a high energy level (3.2 V vs.  $K^+/K$ ), which is much higher (+1.45 V) than that observed in the case of nanosized  $\alpha$ - $V_2O_5$ , showing a much easier insertion process. Furthermore, a

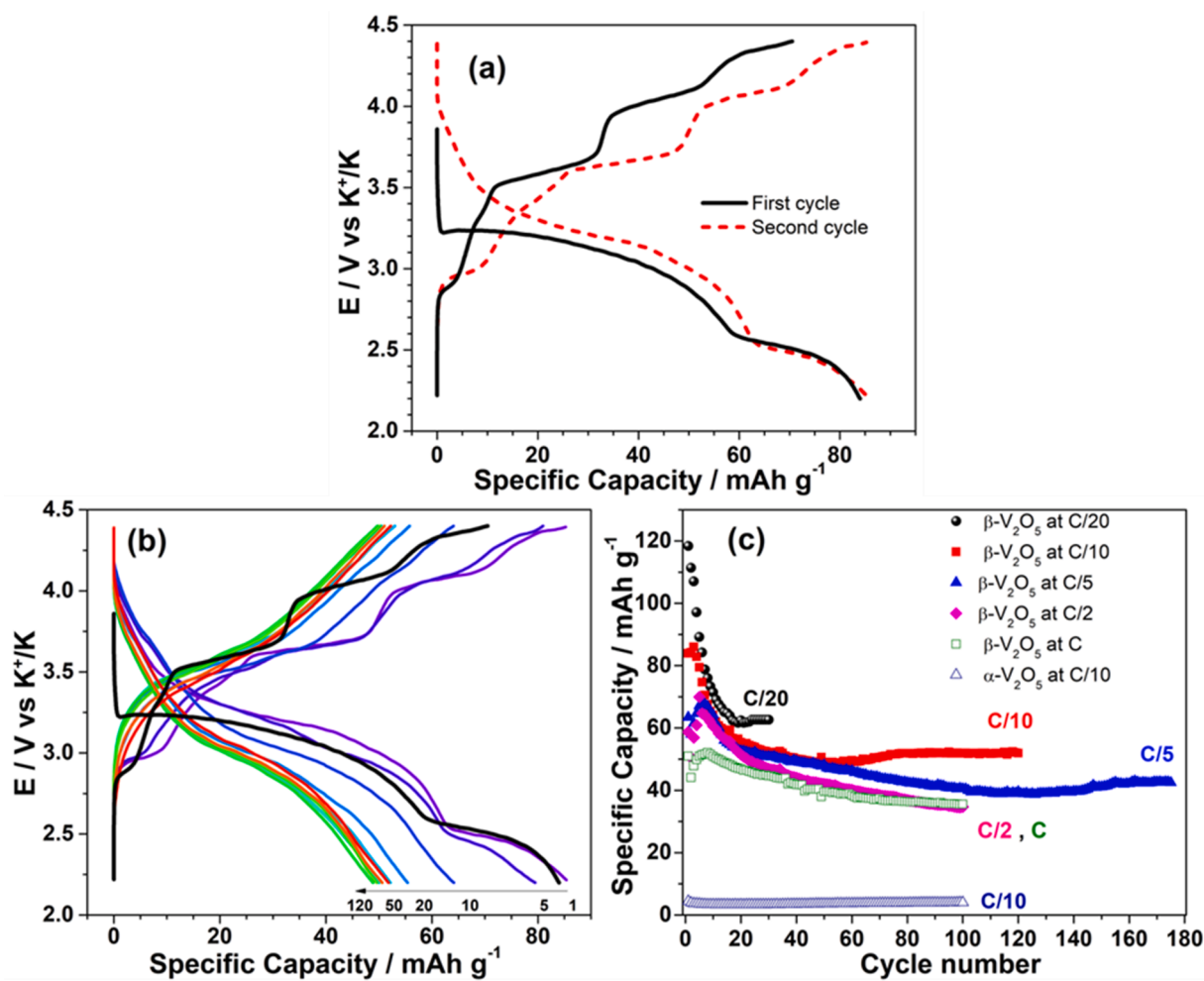


Fig. 3. Electrochemical performance of  $\beta\text{-V}_2\text{O}_5$  (a) First and second discharge-charge cycles at C/10 rate; (b) Discharge-charge cycles from cycle 1 to 120 at C/10 rate; (c) Evolution of the specific capacity upon cycling at different C-rates. 2.2–4.4 V voltage window. 0.5 M KPF<sub>6</sub> EC: PC + 2% FEC electrolyte.

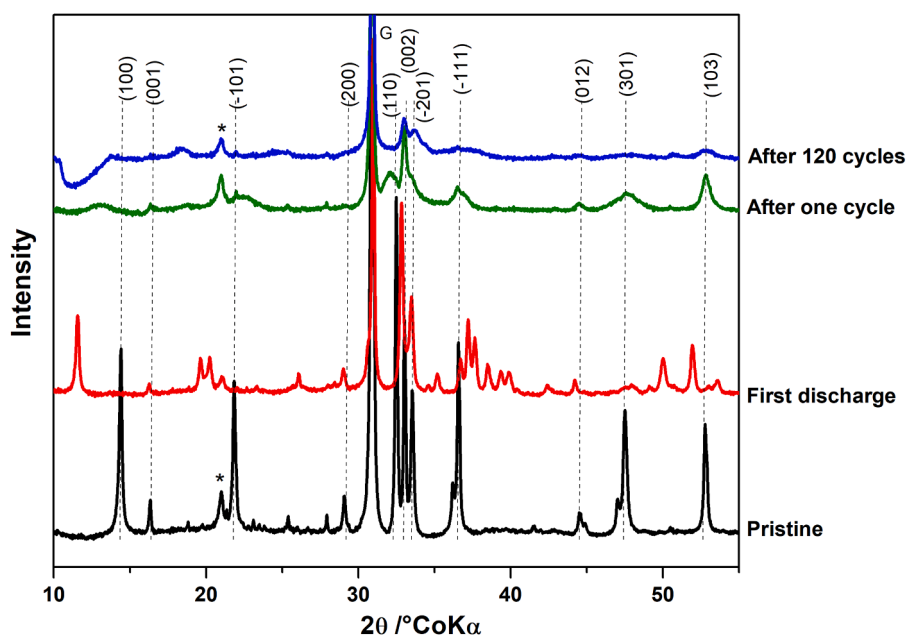


Fig. 4. XRD patterns of the pristine electrode, after first discharge till 2.2 V leading to  $\text{K}_{0.8}\text{V}_2\text{O}_5$  composition (red), after first discharge-charge cycle (green) and after 120 cycles (black). \*: PTFE reflection. G: Graphite line.

twofold specific discharge capacity is reached in the same voltage range. The superior electrode characteristics of the  $\beta$ - $V_2O_5$  polymorph compared to the ambient pressure polymorph have been previously discussed [22,23]. The electrical conductivity of the electrode material is crucial for the kinetics of the intercalation reaction, therefore governing the polarization of the positive electrode and the power rate capability of the lithium cell. To the best of our knowledge there are no reports comparatively investigating the ionic conductivity in the layered structures of the two polymorphs. Regarding the electronic conductivity, the measured resistivities at room temperature are  $10,000 \Omega \text{ cm}$  in  $\alpha$ -polymorph vs.  $400 \Omega \text{ cm}$  in the  $\beta$ -polymorph [22]. The enhanced electronic conductivity of HP- $V_2O_5$  with respect to that of the ambient pressure form is a major advantage in terms of electrochemical performance.

A deep structural investigation is required for understanding the electrochemical properties of  $\beta$ - $V_2O_5$  and in particular the structural pathways for the phase transformations upon discharge and charge as well as the crucial role of the last step at 2.6 V on the cycling behaviour.

A first insight into the structural changes occurring in  $\beta$ - $V_2O_5$  upon potassium insertion can be given by analyzing the ex-situ XRD patterns and Raman spectra recorded at the end of the first discharge at 2.2 V (corresponding to  $K_{0.8}V_2O_5$  composition), after first charge and 120th charge (Figs. 4 and 5, respectively). Upon the first reduction (0.8 K), a significant shift of the (100) diffraction peak to lower angles is observed (Fig. 4), which is associated with an elongation in the  $a$  axis from 7.1 to  $\sim 9 \text{ \AA}$  induced by  $K^+$  insertion in the interlayer space. A similar

phenomenon was reported to take place for Mg [21] and in a larger extent for Na [20] insertion ( $a = 10.097 \text{ \AA}$  for 0.7 Na). Upon the first oxidation, most of the reflections of  $\beta$ - $V_2O_5$  are recovered with however the disappearance of the lowest angle (100) peak and a broadening of the lines suggesting some amorphization upon  $K^+$  deinsertion. This disordering process is all the more marked after 120 discharge-charge cycles but the structure of  $\beta$ - $V_2O_5$  seems to be retained, which account for the good cycling stability evidenced above.

Raman spectroscopy experiments reveal also significant changes upon the first K ion insertion (first discharge, see Fig. 5). Indeed, the bands in the low frequency region are still visible but become weak and broad, suggesting a disordered character in spite of the retaining of the local structure of the chains when moving from  $\beta$ - $V_2O_5$  to  $K_{0.8}V_2O_5$ . The high frequency band features undergo significant intensity and frequency variation. The  $1017 \text{ cm}^{-1}$  peak assigned to the vibration of the terminal  $V_a-O_{1a}$  bond disappears while an intense new band appears at  $890 \text{ cm}^{-1}$  with a shoulder at  $855 \text{ cm}^{-1}$ . Two new components are also seen in the region corresponding to the vibrations of the bridging  $O_3$  atoms at  $772$  and  $527 \text{ cm}^{-1}$ . These observations are consistent with  $K^+$  ions insertion in the interlayer space of  $V_2O_5$  impacting the V-O bonding in the vicinity of the terminal  $O_{1a}$  and bridging  $O_3$  atoms while  $O_{2a}/O_{2b}$  atoms vibrations located in the chains are little affected (Fig. S1). The important frequency shift of the  $V_a-O_{1a}$  vibration ( $\Delta\nu = -130 \text{ cm}^{-1}$ ) suggests a significant lengthening of this bond upon  $K^+$  insertion. After the first cycle, it is remarkable to observe again the Raman fingerprint of the pristine material with only slight alteration in the high frequency

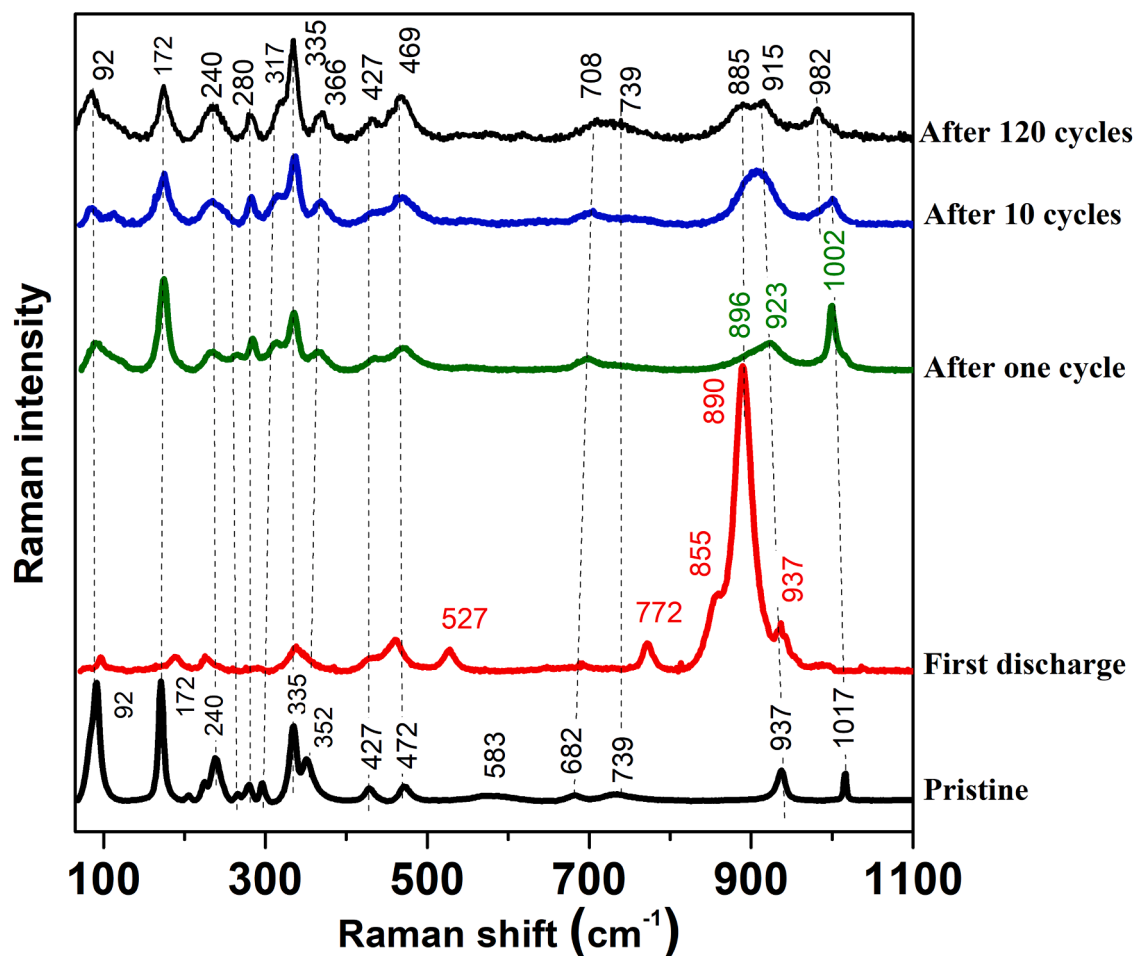


Fig. 5. Raman spectra of the initial electrode, after first discharge till 2.2 V leading to  $K_{0.8}V_2O_5$  composition (red), after first discharge-charge cycle (green), after 10 cycles (blue) and after 120 cycles (black).

region. This comment is also true when looking at the Raman spectra after 10 and 120 cycles, showing the structural reversibility at the atomic scale of the transformation upon several  $K^+$  insertion-deinsertion reactions.

These preliminary ex-situ structural characterization reveal an overall reversible  $K^+$  insertion/extraction process, that leads back to the pristine phase. This contrasts with the irreversible potassiation process previously reported in the case of nanosized  $\alpha\text{-V}_2\text{O}_5$  [15]. Work is in progress to elucidate the detailed mechanism of  $K^+$  intercalation/deintercalation in HP- $\text{V}_2\text{O}_5$ .

#### 4. Conclusion

Reversible potassium insertion into layered  $\beta\text{-V}_2\text{O}_5$  host is reported here for the first time. Phase-pure  $\beta\text{-V}_2\text{O}_5$  is synthesized by subjecting commercial  $\alpha\text{-V}_2\text{O}_5$  at a high pressure and temperature. Potassium ion intercalation properties of monoclinic type  $\beta\text{-V}_2\text{O}_5$  structure are confirmed by EDS, XRD and Raman analyses.  $\beta\text{-V}_2\text{O}_5$  polymorph shows reversible  $K^+$ -ion deinsertion involving multiple stepwise voltage profiles leading to a discharge capacity of 120 mAh  $\text{g}^{-1}$  at C/20 rate corresponding to the  $\text{K}_{0.8}\text{V}_2\text{O}_5$  composition at a mid-discharge potential of 3.2 V vs.  $K^+/K$ . The  $\beta\text{-V}_2\text{O}_5$  system overpasses the parent  $\alpha\text{-V}_2\text{O}_5$  phase in terms of specific capacity and working voltage and competes with the  $\gamma\text{-V}_2\text{O}_5$  polymorph and the best bilayered KVO [27]. Preliminary cycling tests show stable capacities of 60 and 50 mAh  $\text{g}^{-1}$  at C/20 and C/10 respectively over tens of cycles. However, further studies are required to understand the structural changes and the  $K^+$  diffusion process in  $\beta\text{-V}_2\text{O}_5$  in order to improve its rate capability and cycling properties. As a result,  $\beta\text{-V}_2\text{O}_5$  can be proposed as a suitable host material for  $K^+$ -ion insertion with superior performance than the parent  $\alpha\text{-V}_2\text{O}_5$ . This study confirms once more the richness of polymorphism in the  $\text{V}_2\text{O}_5$  system in terms of insertion properties and electrochemical behavior.

#### CRedit authorship contribution statement

**Ankush Bhatia:** Writing – review & editing, Writing – original draft, Visualization, Validation, Methodology, Investigation, Conceptualization. **Jean-Pierre Pereira-Ramos:** Validation, Supervision, Funding acquisition, Conceptualization. **Maria Elena Arroyo-de Dompablo:** Validation, Resources. **Rita Baddour-Hadjean:** Writing – review & editing, Writing – original draft, Validation, Supervision, Project administration, Methodology, Funding acquisition, Conceptualization.

#### Declaration of competing interest

The authors declare that they have no known competing financial interests or personal relationships that could have appeared to influence the work reported in this paper.

#### Data availability

Data will be made available on request.

#### Supplementary materials

Supplementary material associated with this article can be found, in the online version, at [doi:10.1016/j.electacta.2024.144311](https://doi.org/10.1016/j.electacta.2024.144311).

#### References

- W. Luo, J. Wan, B. Ozdemir, W. Bao, Y. Chen, J. Dai, L. Hu, Potassium ion batteries with graphitic materials, *Nano Lett.* 15 (2015) 7671–7677, <https://doi.org/10.1021/acs.nanolett.5b03667>.
- S. Komaba, T. Hasegawa, M. Dahbi, K. Kubota, Potassium intercalation into graphite to realize high-voltage/high-power potassium-ion batteries and potassium-ion capacitors, *Electrochem. Commun.* 60 (2015) 172–175, <https://doi.org/10.1016/j.elecom.2015.09.002>.
- T. Hosaka, K. Kubota, A.S. Hameed, S. Komaba, Research development on K-Ion batteries, *Chem. Rev.* 120 (2020) 6358–6466, <https://doi.org/10.1021/acs.chemrev.9b00463>.
- H. Kim, J.C. Kim, M. Bianchini, D.H. Seo, J. Rodriguez-Garcia, G. Ceder, Recent progress and perspective in electrode materials for K-Ion batteries, *Adv. Energy Mater.* 8 (2018) 1–19, <https://doi.org/10.1002/aenm.201702384>.
- X. Xu, F. Xiong, J. Meng, X. Wang, C. Niu, Q. An, L. Mai, Vanadium-based nanomaterials: a promising family for emerging metal-ion batteries, *Adv. Funct. Mater.* 30 (2020) 1–36, <https://doi.org/10.1002/adfm.201904398>.
- J.P. Pereira-Ramos, R. Messina, J. Perichon, Electrochemical formation of vanadium pentoxide bronzes  $\text{M}_x\text{V}_2\text{O}_5$  in molten dimethylsulfone, *J. Electrochem. Soc.* 135 (1988) 3050–3057, <https://doi.org/10.1149/1.2095486>.
- L. Deng, X. Niu, G. Ma, Z. Yang, L. Zeng, Y. Zhu, L. Guo, Layered potassium vanadate  $\text{K}_{0.5}\text{V}_2\text{O}_5$  as a cathode material for nonaqueous potassium ion batteries, *Adv. Funct. Mater.* 28 (2018) 1800670, <https://doi.org/10.1002/adfm.201800670>.
- Y. Zhang, X. Niu, L. Tan, L. Deng, S. Jin, L. Zeng, H. Xu, Y. Zhu,  $\text{K}_{0.83}\text{V}_2\text{O}_5$ : a new layered compound as a stable cathode material for potassium-ion batteries, *ACS Appl. Mater. Interfaces* 12 (2020) 9332–9340, <https://doi.org/10.1021/acsami.9b22087>.
- X. Liu, G.A. Elia, X. Gao, B. Qin, H. Zhang, S. Passerini, Highly concentrated KTFSS: glyme electrolytes for K/Bilayered- $\text{V}_2\text{O}_5$  batteries, *Batter. Supercaps.* 3 (2020) 261–267, <https://doi.org/10.1002/batt.202000003>.
- B. Tian, W. Tang, C. Su, Y. Li, Reticular  $\text{V}_2\text{O}_5 \cdot 0.6\text{H}_2\text{O}$  xerogel as cathode for rechargeable potassium ion batteries, *ACS Appl. Mater. Interfaces* 10 (2018) 642–650, <https://doi.org/10.1021/acsami.7b15407>.
- M. Clites, J.L. Hart, M.L. Taheri, E. Pomerantseva, Chemically preintercalated bilayered  $\text{K}_x\text{V}_2\text{O}_5$  in  $\text{H}_2\text{O}$  nanobelts as a high-performing cathode material for K-Ion batteries, *ACS Energy Lett.* 3 (2018) 562–567, <https://doi.org/10.1021/acscenergylett.7b01278>.
- A. Eftekhari, Potassium secondary cell based on Prussian blue cathode, *J. Power Sources* 126 (2004) 221–228, <https://doi.org/10.1016/j.jpowsour.2003.08.007>.
- X. Jiang, T. Zhang, L. Yang, G. Li, J.Y. Lee, A Fe/Mn-based prussian blue analogue as a K-Rich cathode material for potassium-ion batteries, *ChemElectroChem.* 4 (2017) 2237–2242, <https://doi.org/10.1002/celec.201700410>.
- K. Chihara, A. Katogi, K. Kubota, S. Komaba,  $\text{KVPO}_4\text{F}$  and  $\text{KVOPO}_4$  toward 4 V-class potassium-ion batteries, *Chem. Commun.* 53 (2017) 5208–5211, <https://doi.org/10.1039/C6CC10280H>.
- Q. Fu, A. Sarapulova, L. Zhu, G. Melinte, A. Missyul, E. Welter, X. Luo, M. Knapp, H. Ehrenberg, S. Dsoke, In operando study of orthorhombic  $\text{V}_2\text{O}_5$  as positive electrode materials for K-ion batteries, *J. Energy Chem.* 62 (2021) 627–636, <https://doi.org/10.1016/j.jechem.2021.04.027>.
- P. Vishnuprakash, C. Nithya, M. Premalatha, Exploration of  $\text{V}_2\text{O}_5$  nanorod/rGO heterostructure as potential cathode material for potassium-ion batteries, *Electrochim. Acta* 309 (2019) 234–241, <https://doi.org/10.1016/j.electacta.2019.04.092>.
- F. Ye, D. Lu, X. Gui, T. Wang, X. Zhuang, W. Luo, Y. Huang, Atomic layer deposition of core-shell structured  $\text{V}_2\text{O}_5$ @CNT sponge as cathode for potassium ion batteries, *J. Mater.* 5 (2019) 344–349, <https://doi.org/10.1016/j.jmat.2018.05.009>.
- A. Bhatia, J.-P. Pereira-Ramos, N. Emery, R. Baddour-Hadjean,  $\gamma\text{-V}_2\text{O}_5$  polymorph as a promising host structure for potassium ion battery: an electrochemical and structural study, *Chem. Mater.* 33 (2021) 5276–5289, <https://doi.org/10.1021/ACS.CHEMMATER.1C01390>.
- M.E. Arroyo y de Dompablo, J.M. Gallardo-Amores, U. Amador, E. Morán, Are high pressure materials suitable for electrochemical applications? HP- $\text{V}_2\text{O}_5$  as a novel electrode material for Li batteries, *Electrochem. Commun.* 9 (2007) 1305–1310, <https://doi.org/10.1016/j.elecom.2007.01.035>.
- R. Córdoba, A. Kuhn, J.C. Pérez-Flores, E. Morán, J.M. Gallardo-Amores, F. García-Alvarado, Sodium insertion in high pressure  $\beta\text{-V}_2\text{O}_5$ : a new high capacity cathode material for sodium ion batteries, *J. Power Sources* 422 (2019) 42–48, <https://doi.org/10.1016/j.jpowsour.2019.03.018>.
- R. Trócoli, P. Parajuli, C. Frontera, A.P. Black, G.C.B. Alexander, I. Roy, M. E. Arroyo-De Dompablo, R.F. Klie, J. Cabana, M.R. Palacín,  $\beta\text{-V}_2\text{O}_5$  as Magnesium Intercalation Cathode, *ACS Appl. Energy Mater.* 5 (2022) 11964–11969, <https://doi.org/10.1021/acsaem.2c02371>.
- J.M. Gallardo-Amores, N. Biskup, U. Amador, K. Persson, G. Ceder, E. Morán, M. E. Arroyo y de Dompablo, Computational and experimental investigation of the transformation of  $\text{V}_2\text{O}_5$  under pressure, *Chem. Mater.* 19 (2007) 5262–5271, <https://doi.org/10.1021/cm071360p>.
- M.E.A. Dompablo, U. Amador, J.M. Gallardo-Amores, C. Baetz, N. Biskup, E. Morán, High pressure materials for energy storage: the case of  $\text{V}_2\text{O}_5$ , *J. Phys. Conf. Ser.* 121 (2008) 032001, <https://doi.org/10.1088/1742-6596/121/3/032001>.
- V.P. Filonenko, M. Sundberg, P.E. Werner, I.P. Zibrov, Structure of a high-pressure phase of vanadium pentoxide,  $\beta\text{-V}_2\text{O}_5$ , *Acta Crystallogr. Sect. B Struct. Sci.* 60 (2004) 375–381, <https://doi.org/10.1107/S0108768104012881>.
- R. Baddour-Hadjean, M.B. Smirnov, K.S. Smirnov, V.Y. Kazimirov, J.M. Gallardo-Amores, U. Amador, M.E. Arroyo-De Dompablo, J.P. Pereira-Ramos, Lattice dynamics of  $\beta\text{-V}_2\text{O}_5$ : raman spectroscopic insight into the atomistic structure of a

- high-pressure vanadium pentoxide polymorph, *Inorg. Chem.* 51 (2012) 3194–3201, <https://doi.org/10.1021/ic202651b>.
- [26] A. Bhatia, J.P. Pereira-Ramos, N. Emery, B. Laik, R.I. Smith, R. Baddour-Hadjean, An exploratory investigation of spinel  $\text{LiMn}_{1.5}\text{Ni}_{0.5}\text{O}_4$  as cathode material for potassium-ion battery, *ChemElectroChem* (2020) 1–10, <https://doi.org/10.1002/celec.202000889>.
- [27] Y.-H. Zhu, Q. Zhang, X. Yang, E.-Y. Zhao, T. Sun, X.-B. Zhang, S. Wang, X.-Q. Yu, J.-M. Yan, Q. Jiang, Reconstructed orthorhombic  $\text{V}_2\text{O}_5$  polyhedra for fast ion diffusion in K-ion batteries, *Chem* 5 (2019) 168–179, <https://doi.org/10.1016/j.chempr.2018.10.004>.